Chemoselective Liquid Phase Hydrogenation of 3-Nitrostyrene over Pt Nanoparticles: Synergy with ZnO Support

ARTICLE *in* INDUSTRIAL & ENGINEERING CHEMISTRY RESEARCH · SEPTEMBER 2015

Impact Factor: 2.59 · DOI: 10.1021/acs.iecr.5b02113

I&EC research
Industrial & Engineering Chemistry Research

Article

pubs.acs.org/IECR

Chemoselective Liquid Phase Hydrogenation of 3-Nitrostyrene over Pt Nanoparticles: Synergy with ZnO Support

Charline Berguerand,[†] Artur Yarulin,[†] Fernando Cárdenas-Lizana,[†] Johan Wärnå,[‡] Esther Sulman,[§] Dmitry Yu. Murzin,*[,‡] and Lioubov Kiwi-Minsker*[,†,⊥]

[†]Group of Catalytic Reaction Engineering, Ecole Polytechnique Fédérale de Lausanne, Station 6, Lausanne CH-1015, Switzerland
[‡]Åbo Akademi University, Turku/Åbo 20500, Finland
[§]Department of Biotechnology and Chemistry, Tver Technical University, Tver 170026, Russian Federation
[⊥]Regional Technological Centre, Tver State University, Tver 170100, Russian Federation

Supporting Information

ABSTRACT: Hydrogenation of 3-nitrostyrene was performed at T = 348 K and 10 bar over platinum nanoparticles supported on several metal oxides. Pt/Al_2O_3 and Pt/C catalysts exhibited high activity giving 3-ethylaniline as the only product, while Pt/ZnO displayed high selectivity toward target 3-vinylaniline at close to full substrate conversion due to PtZn alloy formation. The catalyst also showed a robust behavior without detectable catalyst deactivation in repeated reaction runs. The most suitable solvent for this reaction was ethanol. Kinetic modeling for nitrostyrene hydrogenation was successfully performed based on the proposed parallel-consecutive reaction network. Application of Pt/ZnO for hydrogenation of various 3-substituted (−CH_3, −H, −Cl, −Br, −$CHCH_2$, −COOH, and −NO_2) nitroarenes resulted in almost exclusive formation of the corresponding amino-compounds.

INTRODUCTION

Selective catalytic hydrogenation of organic molecules is one of the most important processes in fine chemistry and pharmaceuticals.[1] Functionalized anilines produced by reduction of corresponding nitroarenes are intermediates in the manufacturing of many agrochemicals, pharmaceuticals, dyes, and pigments.[2,3] An effective catalyst developed by Ciba-Geigy for herbicide intermediates production allows >99% selectivity toward the desired aniline, but only with the addition of modifiers.[5] The presence of additives, even in small concentration, could affect product purity. Therefore, an alternative approach is to introduce modifiers into the catalyst formulation.[4,6]

Among the functionalized anilines, 3-vinylaniline (3-VA) is a key compound for the production fine chemicals[7,8] and functionalized polymers.[9,10] 3-VA is normally produced by hydrogenation of 3-nitrosytrene (3-NS). Because of the presence of an easily reducible vinyl-group, the reaction chemoselectivity is a key issue in this process. The reaction network of 3-NS hydrogenation is similar to that proposed by Haber for nitrobenzene reduction (Scheme 1).[11] Two different reaction routes to 3-VA are suggested:[12] the direct paths via the pathway **1** and the condensation route via paths **5** and **6**.

3-NS hydrogenation is typically carried out in organic solvents, such as toluene and tetrahydrofuran,[13,14] with serious implications in terms of environmental impact.[15] High selectivity (up to 99%) in terms of exclusive nitro-group hydrogenation, but low activity (~170 mol mol_{Me}^{-1} h^{-1}), has been reported for 3-NS hydrogenation over the Au/TiO_2 catalyst (P_{H2} = 3 bar, T = 393 K).[14] Higher hydrogenation rates (~3000 mol mol_{Me}^{-1} h^{-1}) were achieved over Pt/TiO_2, but an appreciable formation of byproducts ($S_{3\text{-VA}} \leq 93\%$) was detected.[13]

Scheme 1. Reaction Scheme for the 3-Nitrosytrene Hydrogenation

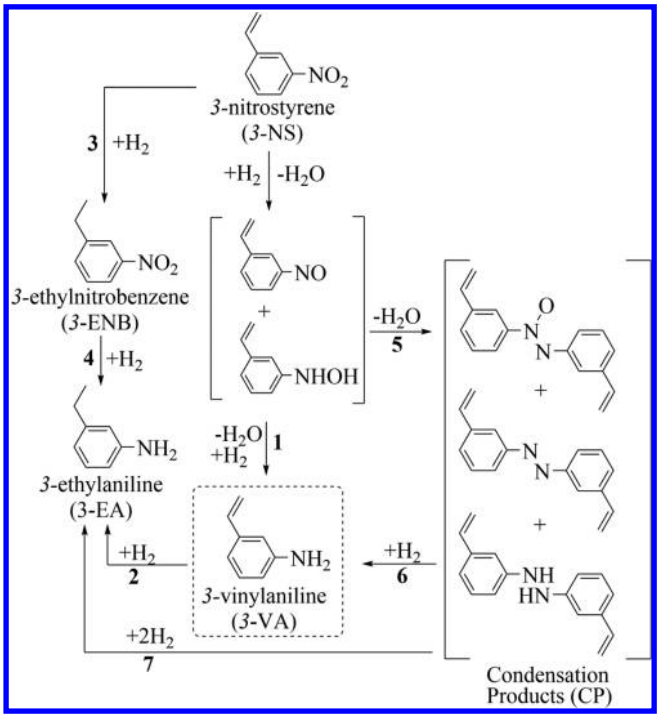

Received: June 11, 2015
Revised: August 12, 2015
Accepted: August 14, 2015
Published: August 14, 2015

DOI: 10.1021/acs.iecr.5b02113
Ind. Eng. Chem. Res. 2015, 54, 8659−8669

The use of zinc as modifier into the catalyst formulation permits to diminish C=C double bond hydrogenation. Silvestre-Albero et al.[16] suggested that the change of electronic properties of Pt in PtZn alloy hinders the adsorption of C=C double bond during crotonaldehyde hydrogenation. The same effect of diminished C=C double bond hydrogenation upon formation of PdZn was reported by Crespo-Quesada et al.[17] This observation could be used to prevent the adsorption of the vinyl group present on 3-NS.

By taking into consideration the above-mentioned findings as well as the promising catalytic performance for nitro-group reduction over Pt nanoparticles,[18,19] in the current work, selective hydrogenation of a series of substituted nitroarenes was carried out using Pt−Zn catalytic system. Our previous work for Pt promoted with Zn of the size about 4.7 nm confined in the polymer (hyper-cross-linked polystyrene, HPS) matrix demonstrated that a substantial six-fold activity boost in nitrostyrene hydrogenation can be achieved for this Pt−Zn/HPS catalyst compared to monometallic Pt/HPS. However, formation of catalytically active sites $Pt^{\delta-}$−$Zn^{\delta+}$ because of Pt alloying with Zn when ZnO was used as a support was described in the literature[20] leading to enhanced selectivity in hydrogenation of crotonaldehyde. Inspired by these studies, in the current work, Pt nanoparticles were supported on ZnO and tested in hydrogenation of substituted nitroarenes with a special emphasis on 3-NS.

Pt/ZnO has been compared with two commercial catalysts, namely Pt supported on activated carbon (Pt/C) and on Al_2O_3 (Pt/Al_2O_3). Moreover, Pt nanoparticles supported on a series of oxides (MgO, CeO_2, TiO_2, and Fe_2O_3) was also tested. The catalysts have been characterized by different physicochemical methods. The reaction kinetics study based on the advanced reaction mechanism was also performed.

EXPERIMENTAL SECTION

Materials. The chemicals, nitrobenzene (99%, Acros), 3-NS (99%, Acros), 3-nitrotoluene (99%, Aldrich), 3-chloronitrobenzene (98%, Alfa Aesar), 3-bromonitrobenzene (97%, Aldrich), 3-nitrobenzoic acid (98%, Aldrich), 3-dinitrobenzene (99%, TCI), and solvents, toluene, (99%, Fisher Scientific), isopropanol (98%, Aldrich), acetonitrile (99%, Fisher Scientific), ethanol (95%, Aldrich), methanol (99%, Acros), tetrahydrofuran (99%, Fisher Scientific), and butanol (99%, Fisher Scientific) were used as received without purification. All the gases employed in this work (H_2, N_2, Ar, CO, and He) were of ultrahigh purity (>99.99%, Carbagas).

Catalyst Preparation. The as-received oxides used as supports were first crashed in a centrifugal ball (2 cm; ágat) mill (Fritsch Pulverisette 6) working with a rotation speed of about 90 rpm and sieved into a batch of 60−100 μm average particle diameter. The Pt/MeO_x catalysts were prepared by incipient wetness impregnation as described in the following.

The Pt/ZnO catalyst was prepared as follows: 5 mL of a 0.128 M aqueous solution of hexachloroplatinic acid (H_2PtCl_6) was added to 100 mL of an aqueous suspension containing 10 g of ZnO (>99.9%, Aldrich), and the mixture was stirred for 24 h at room temperature. Then the solid was filtered, washed with H_2O and ethanol, and dried overnight at room temperature. The reduction was performed by hydrogen (10% vol. in Ar, 340 mL min^{-1}, temperature ramp of 5 K min^{-1}) at desired temperature maintained 2 h. Finally, the catalyst was cooled down to room temperature under inert (Ar) flow.

Pt/MgO, Pt/CeO_2, Pt/Fe_2O_3, and Pt/TiO_2 catalysts were prepared following the same procedure but using magnesium oxide (>98%, Fluka), cerium oxide (99.9%, Acros), iron oxide (>99%, Fluka), and titanium oxide (>99%, Sigma) as supports.

The catalysts were designated Pt/MO_x-T, where MO_x is the metal oxide support, and T is the reduction temperature (e.g., Pt/ZnO-473). If no reduction temperature is mentioned, it means that the catalyst was reduced at 573 K.

Catalyst Characterization. The Pt content in the catalysts was determined by atomic absorption spectroscopy (AAS) using a Shimadzu AA-6650 spectrometer with an air-acetylene flame after catalyst dissolution in aqua regia (25% v/v HNO_3/HCl). Pt leaching that can take place during the catalytic hydrogenations was controlled by means of (i) comparison of Pt content in the catalyst before and after the reaction, (ii) AAS analysis of the final reaction solution after the catalyst separation by filtration, and (iii) carrying out the hydrogenation reaction reusing the final reaction solution after the catalyst separation with the addition of the substrate. In the last-mentioned case, any detected conversion could indicate Pt leaching during the catalytic reaction.

Brunauer−Emmett−Teller (BET) surface area was determined using the commercial Sorptomatic 1990 (Carlo Erba). Prior to analysis, the samples were outgassed at 523 K for 2 h under vacuum ($<5 \times 10^{-2}$ Torr). BET surface area was obtained by nitrogen adsorption−desorption at 77 K according to the method of Dollimore and Heal.[21] The BET surface areas were reproducible to within ±6%, and the values quoted in this study are the mean ones.

Temperature-programmed reduction (TPR) in hydrogen and CO chemisorption was carried out using a commercial AutoChem II unit (Micromeritics). The samples were loaded into a U-shaped Quartz cell (10 mm i.d.) and heated in a 10% v/v H_2/N_2 gaseous mixture flow (20 cm^3 min^{-1}; Brooks mass flow controllers) at a temperature ramp of 5 K min^{-1} to 573 K. The effluent gas passed through a liquid N_2+isopropanol trap, and the H_2 consumption was monitored by a thermal conductivity detector (TCD) with data acquisition/manipulation using Autochem II 2920 V3.03 software. The reduced samples were maintained at the final temperature in a H_2 flow until the TCD signal returned to baseline, was swept with a 65 cm^3 min^{-1} flow of N_2 for 1.5 h, cooled to 323 K, and subjected to CO chemisorption using a pulse (300 μL) titration procedure. In a blank test, chemisorption measurements on ZnO support did not result in any detectable CO uptake.

The Pt nanoparticle size was determined by a transmission electron microscopy (TEM) using Philips FEI CM12 TEM microscope operated at an accelerating voltage of 120 kV employing Gatan Digital Micrograph 1.82 for data acquisition/manipulation. The specimens were prepared by dispersion in ethanol and deposited on a holey carbon/Cu grid (300 Mesh). Up to 300 individual Pt nanoparticles were counted for each catalyst, and the number-average diameter (d) was calculated from

$$d = \frac{\sum_i n_i d_i}{\sum_i n_i} \quad (1)$$

where n_i is the number of particles of diameter d_i. The size limit for the detection is about 1 nm.

Powder X-ray diffractograms (XRD) were recorded on a Bruker/Siemens D500 incident X-ray diffractometer (Cu Kα radiation) and identified against JCPDS-ICDD standards. The

DOI: 10.1021/acs.iecr.5b02113
Ind. Eng. Chem. Res. 2015, 54, 8659−8669

samples were scanned at a rate of 0.02° step^{-1} over the range 20° ≤ 2θ ≤ 90° (scan time = 1 s step^{-1}).

X-ray photoelectron spectroscopy (XPS) analyses were conducted using an Axis Ultra instrument (Kratos Analytical) under ultrahigh vacuum conditions (<10^{-8} Torr) with a monochromatic Al Kα X-ray source (1486.6 eV). The source power was maintained at 150 W, and the emitted photoelectrons were sampled from a 750 × 350 μm^2 area at a takeoff angle = 90°. The analyzer pass energy was 80 eV for survey spectra (0−1000 eV) and 40 eV for high-resolution spectra (Pt 4$f_{5/2}$ and 4$f_{7/2}$). The adventitious carbon C 1s peak was calibrated at 284.5 eV and used as an internal standard to compensate any charging effects.[22] Spectra curve fitting and quantification were performed with the CasaXPS software using relative sensitivity factors provided by Kratos.

Catalytic System and Reaction Procedure. Liquid phase hydrogenation reactions (T = 313−393 K; P = 1−15 bar) were carried out in a commercial semibatch stirred stainless steel reactor (100 cm^3 autoclave, Büchi AG, Uster, Switzerland) equipped with a pressure-controlled H_2 supply system (Büchi pressflow gas controller bpc 6002, Büchi AG, Uster, Switzerland). A stainless steel six-blade disk turbine (equipped with a self-gassing hollow shaft) provided effective agitation at 1500 rpm. A heat exchanger with a cooling system (Haake B−N2) was used to control the reaction temperature within ±1 K using oil (Shell Thermia; thermal conductivity = 0.45 kJ m^{-1} h^{-1} K^{-1}; specific heat = 2.4 kJ kg^{-1} K^{-1}) as a thermal medium. At the beginning of each experiment, 80 mL of nitroarene solution with an initial concentration of 2.5 × 10^{-5} mol/cm^3 and a catalyst were charged into the reactor and flushed three times with N_2 to remove any reacting gases from the reactor. The system was then heated up to the reaction temperature under continuous stirring (ca. 800 rpm) at which point hydrogen was introduced. The system was pressurized and intensive stirring (>1500 rpm), to avoid any external mass transfer limitations,[23] was engaged (time t = 0 for the reaction). The initial substrate to Pt ratio spanned the range from 100−150 $mol_{3\text{-NC}}$ mol_{Pt}^{-1}. A liquid sampling system via a syringe with in-line filters allowed a controlled withdrawing of aliquots (≤0.25 cm^3) from the reactor. Repeated reaction runs with the same catalyst batch delivered conversion/selectivity values that were reproducible to within ±5%. In a series of blank tests, no measurable conversion was detected for reactions carried out in the absence of catalyst or in the presence of ZnO support alone, that is, without Pt.

The composition of the reaction media was analyzed by gas chromatography using a PerkinElmer Clarus 500 chromatograph equipped with a programmed split/splitless injector and a flame ionization detector, employing a Stabilwax (Cross-bond Carbowax-PEG, Restek, USA) capillary column (length 30 m, i.d. = 0.32 mm, film thickness = 0.25 μm). Data acquisition and manipulation were performed using the TotalChrom Workstation (Version 6.3.2 for Windows) data system. The concentration of the organic species in the liquid phase was determined from the total mass balance of the reaction mixture with n-dodecane as internal standard. The conversion of 3-NS ($X_{3\text{-NS}}$) was defined as

$$X_{3\text{-NS}}\ (\%) = \frac{C_{3\text{-NS},0} - C_{3\text{-NS}}}{C_{3\text{-NS},0}} \times 100 \quad (2)$$

and selectivity in terms of 3-VA ($S_{3\text{-VA}}$) as the target product was calculated as

$$S_{3\text{-VA}}\ (\%) = \frac{C_{3\text{-VA}}}{C_{3\text{-NS},0} - C_{3\text{-NS}}} \times 100 \quad (3)$$

Catalyst activity was also quantified in terms of the initial 3-NS consumption rate ($-R_{3\text{-NS},0}$) determined from a linear regression of the temporal 3-NS concentration profile and the turnover frequency (TOF, rate of hydrogenation per active site) obtained from

$$\text{TOF}\ (s^{-1}) = \frac{-R_{3\text{-NS},0} \times M_{Pt}}{D} \quad (4)$$

where M_{Pt} represents the Pt atomic mass, and D is the Pt metal dispersion ($N_{Pt,surface}$ $N^{-1}_{Pt,total}$) obtained from

$$D\ (-) = \frac{S_{Pt} \times M_{Pt}}{A_{Pt} \times N_A} \quad (5)$$

with A_{Pt} representing the atomic surface ($m_{Pt,surface}^2$ $N_{Pt,surface}^{-1}$) and S_{Pt} the specific metal surface area (m_{Pt}^2 g_{Pt}^{-1}), while N_A is the Avogadro number (6.02 × 10^{23} mol^{-1}).

Finally, the metal surface area was calculated from

$$S_{Pt}\ (m_{Pt}^2 g_{Pt}^{-1}) = \frac{6}{\rho_{Pt} \times d} \quad (6)$$

where ρ_{Pt} = 21.45 g cm^{-3}[24], and d is the average mean Pt particle size determined by TEM analyses.

The Madon-Boudart criterion applied allowed us to ensure the reaction operation under kinetic control.

RESULTS AND DISCUSSION

Catalyst Characterization. To gain a deeper understanding of the source of the distinct catalytic response over the used catalysts, a series of characterization techniques were applied.

Pt Supported on ZnO. The Pt content in the Pt/ZnO catalyst was found to be 1.4 wt % (Table 1). The BET surface area (SSA) of the ZnO support was ∼10 m^2 g^{-1}. This value is in the range of the reported one found elsewhere for different ZnO.[25] The deposition of Pt on the support does not change this characteristic.

Table 1. Physico-Chemical Characteristics of Pt/ZnO Reduced at 573 K

		Pt/ZnO
metal loading (% w/w)		1.4
BET (m^2 g^{-1})		10
TPR T_{max} (K)		406
H_2/Pt (mol mol^{-1})		2.96
d (nm)		2.3[a], 2.8[b]
XPS Pt binding energies (eV)	Pt 4$f_{7/2}$	70.9, 71.9
	Pt 4$f_{5/2}$	74.2, 75.4

[a]Electron microscopy. [b]CO chemisorption.

The TPR profile recorded for ZnO support (Figure 1I) shows no significant hydrogen uptake or release. This observation is in agreement with the thermal stability of ZnO under reductive atmosphere up to 773 K reported elsewhere.[26] The TPR of ZnO modified by H_2PtCl_6 (Figure 1II) demonstrates a sharp peak with a maximum at 406 K. A negative peak in Figure 1 is linked to hydrogen consumption. This peak can be attributed to the reduction of ionic to metallic platinum. A temperature of ∼400 K was assigned to the reduction of oxidized Pt species.[27,28] The H_2(uptake)/Pt molar ratio is in accordance with the trans-

DOI: 10.1021/acs.iecr.5b02113
Ind. Eng. Chem. Res. 2015, 54, 8659−8669

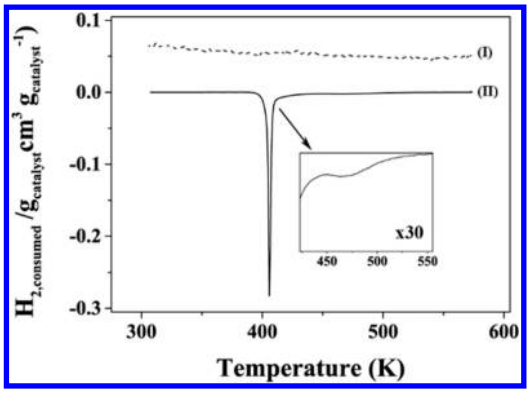

Figure 1. TPR profiles obtained for the reduction of Pt/ZnO (continuous line) and ZnO (dashed line) at the heating rates of 5 K min^{-1}.

formation of $Pt^{4+} \rightarrow Pt^0$ as reported for Pt/Al_2O_3.[28,29] The small reduction peak observed at higher temperature (~450−500 K) can be assigned to Pt-catalyzed reduction of ZnO to metal Zn^0 species, which might form an alloy with Pt. Similar observations were reported by Consonni et al.[20]

The XRD pattern of 2 wt % Pt/ZnO catalyst is shown in Figure S1. The crystallography of zinc oxide is well represented and corresponds to the reference table JCPDS-ICDD 036−145. The position of Pt peaks corresponds to JCPDS-ICDD 001−1190. The position of PtZn alloy peaks corresponds to the reference table JCPDS-ICDD 006−0604. Since the PtZn alloy formation in a Pt/ZnO system is detected,[24,29] XRD analysis of the samples with a higher Pt loading (~5%) or reduced at higher temperatures was also carried out. The presence of PtZn alloy phase is particularly visible for the 5 wt % Pt/ZnO sample reduced at 773 K. Indeed, it is reported elsewhere[30,31] that higher temperature favors the formation of alloy.

To confirm the formation of PtZn alloy, XPS analysis of Pt/ZnO catalyst was carried out. From the overview spectrum (not shown), Zn, O, Pt, and Cl could be identified as components on the surface. By knowing that TPR analysis demonstrated full reduction of Pt, oxygen may be ascribed to its presence in ZnO support and also to oxygen chemisorbed on Pt. The Pt $4f_{7/2}$ spectra of the calcined at 673 K catalyst (Figure 2A) can be deconvoluted into two peak components with binding energies at 70.9 and 72.8 eV. The first peak corresponds to metallic Pt^0 reported at 71.1 ± 0.2 eV.[32] The second peak at 72.8 eV corresponds to oxidized species (PtO) as reported by Hidalgo-Carrillo et al.[24] In the case of the reduced at 573 K catalyst (Figure 2B), the Pt $4f_{7/2}$ spectrum is deconvoluted into the peak at 70.9 eV (metallic Pt^0) and a second peak at 71.9 eV. This second peak with a binding energy higher than that for Pt^0 but lower than that or oxidized PtO species can be attributed to PtZn alloy.

The Pt particle size determined by means of both CO chemisorption (quantification of accessible Pt sites) and electron microscopy is presented in Table 1. The values obtained through both techniques are in a good agreement (2.5 ± 0.3 nm for Pt/ZnO). The high-resolution TEM images and corresponding Pt particle size distribution are presented in Figure 3. The number of counted particles was sufficiently large (ca. 500) to represent correctly the entire particle population according to ref 33. The obtained Pt particle size distribution is quite narrow in the range of 1−6 nm with the significant (ca. 85%) amount of small particles in the range of 1−3 nm.

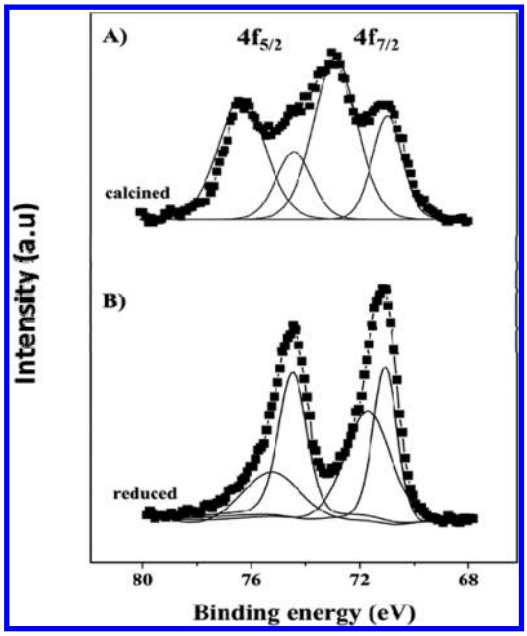

Figure 2. XPS spectrum over the Pt 4*f* region for Pt/ZnO (A) calcined at 573 K and (B) reduced at 573 K.

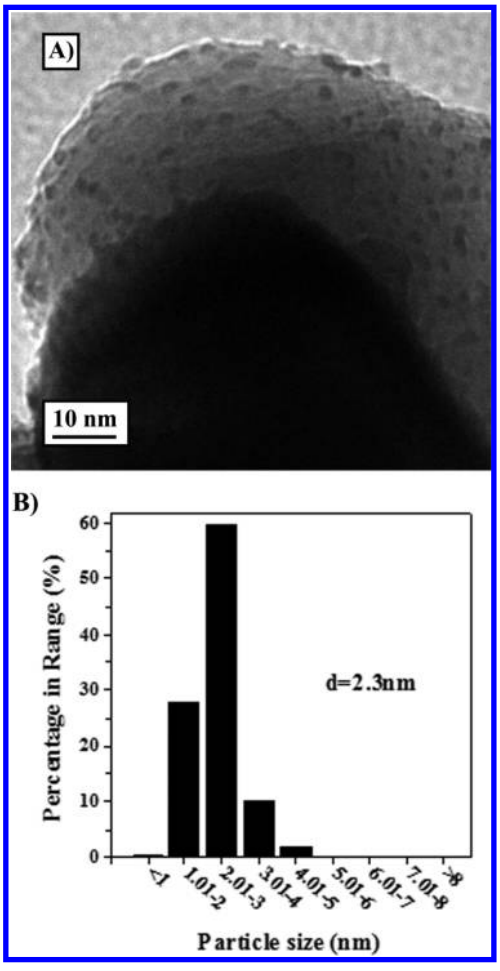

Figure 3. (A) Representative TEM image of Pt nanoparticles deposited on ZnO and (B) particle size distribution for Pt/ZnO.

Pt Supported on Metal Oxides and Carbon. The Pt loadings in the synthesized Pt/MgO, Pt/CeO_2, Pt/Fe_2O_3, and

DOI: 10.1021/acs.iecr.5b02113
Ind. Eng. Chem. Res. 2015, 54, 8659−8669

Pt/TiO_2 catalysts are 0.5, 0.3, 0.2, and 0.1 wt %, respectively. The mean particle sizes determined by CO-chemisorption are 1.8, 3.1, 10.0, 1.0, and 1.4 nm for Pt/Al_2O_3, Pt/MgO, Pt/CeO_2, Pt/Fe_2O_3, and Pt/TiO_2, respectively. The Pt loadings in the commercial Pt/Al_2O_3 and Pt/C catalysts used as reference catalysts were determined to be 0.7 wt % in Pt/Al_2O_3 and 1.0 wt % in Pt/C. The measured BET surface areas (140 $m^2\ g^{-1}$ for Pt/Al_2O_3 and 830 $m^2\ g^{-1}$ for Pt/C) are in the range of the reported value of <250 $m^2\ g^{-1}$ for Pt/Al_2O_3[34] and 209−1140 $m^2\ g^{-1}$ for Pt/C.[33]

Before any use in the catalytic reactions, the benchmark catalysts were treated in hydrogen atmosphere at $T \geq 623$ K for 2 h to activate Pt, as reported for Pt/Al_2O_3[35] and Pt/C.[36] Moreover, to form Pt particles in Pt/C and Pt/Al_2O_3 catalysts in a range of sizes obtained for Pt/ZnO, benchmark catalysts were treated in hydrogen atmosphere at higher temperatures and fixed at 973 and 1123 K, respectively. Representative high-resolution scanning TEM (HR-STEM) images of the treated benchmark Pt/Al_2O_3 and Pt/C are seen in Figure 4. Pt nanoparticles have a

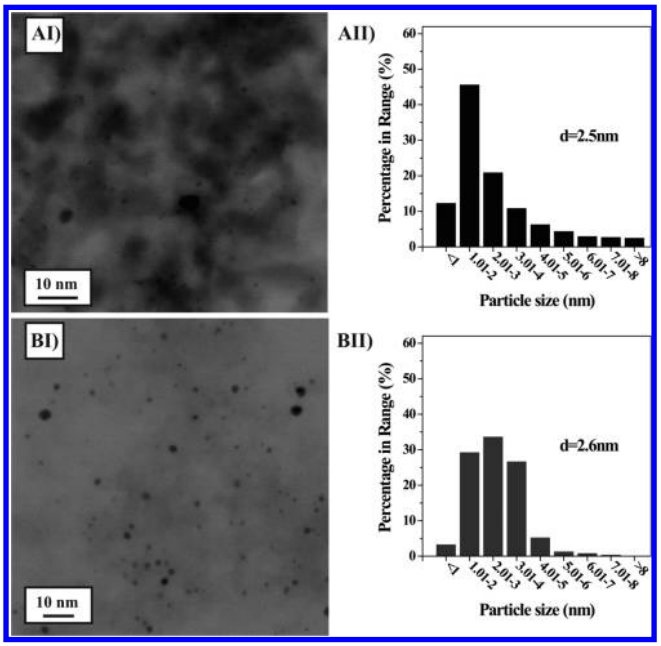

Figure 4. Representative HR-TEM image for benchmark catalysts (A) Pt/Al_2O_3 and (B) Pt/C.

spheroidal shape, consistent with a cuboctahedral crystal morphology, which is the most thermodynamically favorable.[37] In both catalysts, the Pt nanoparticle size distribution is boarder as compared to Pt/ZnO. The mean particle size of 2.5 nm for Pt/Al_2O_3 and 2.6 nm for Pt/C measured through TEM image analysis are close to the value found for the Pt/ZnO (2.5 ± 0.3 nm). These findings are confirmed by CO-chemisorption where the mean particle sizes of 2.7 and 2.9 nm are obtained for Pt/Al_2O_3 and Pt/C, respectively. Although a boarder particle size distribution is obtained for the benchmark catalysts, the close mean particle size found for the Pt/ZnO and treated benchmark catalysts (Pt/Al_2O_3 and Pt/C) allows us to exclude a size effect reported in the literature for nitroarene hydrogenation.[2]

Catalytic Results. To optimize the NS hydrogenation reaction conditions (pretreatment, reaction temperature, pressure, medium, etc.), we investigated each variable independently, and the obtained results are presented in the following sections.

Optimization of Reduction Temperature. The influence of reductive temperature on the Pt/ZnO performance was studied (Table 2). PtZn alloy formation (confirmed by XRD and

Table 2. Catalytic Results in the Liquid-Phase Hydrogenation of 3-NS to 3-VA over Supported Pt Catalysts. Reaction Conditions: 348 K, 10 bar, 3-NS/Pt Molar Ratio = 150 $mol_{3\text{-}NS}$ mol_{Pt}^{-1} with Ethanol as Solvent

catalyst	$S_{3\text{-}VA}$ (%)	$S_{3\text{-}EA}$ (%)	$(-R_{3\text{-}NS})_0 \times 10^{-3}$ ($mol_{3\text{-}NS}\ mol_{Pt}^{-1}\ h^{-1}$)	TOF (s^{-1}) ($mol_{3\text{-}NS}\ mol_{Pt}^{-1}\ h^{-1}$)
	($mol_{3\text{-}NS}\ mol_{Pt}^{-1}\ h^{-1}$)			
Pt/ZnO-473[b]	82	18	0.78	6.2
Pt/ZnO[ab]	97	3	1.56	12.4
Pt/ZnO-673[b]	78	22	0.96	17.0
Pt/ZnO-773[b]	75	15	0.66	20.1
Pt/Al_2O_3[c]	0	100	2.41	21.7
Pt/C[c]	0	100	1.97	18.4
Pt/MgO[b]	0	100	2.57	28.7
Pt/CeO_2[b]	0	100	1.97	68.1
Pt/Fe_2O_3[b]	37	63	1.37	4.7
Pt/TiO_2[b]	53	47	1.39	6.7

[a]Reduced at 573 K. [b]Prepared in our laboratory. [c]Commercial.

XPS) starts at 473 K with H_2PtCl_6 as precursor on ZnO in a H_2 atmosphere.[30] Consonni et al.[20] studied the influence of PtZn alloy formation in Pt/ZnO on the catalyst activity and selectivity. The optimal pretreatment in terms of selectivity and activity is observed at ∼570 K. The reductive treatment performed at temperatures lower than 570 K leads to a partial alloy formation in small Pt nanoparticles. At higher reduction temperatures, Pt nanoparticle agglomeration starts to be important. Indeed, the Pt nanoparticle size in the Pt/ZnO catalyst measured through CO-chemisorption increased from 1.5 nm up to 7.7 nm after an increase of the reductive pretreatment temperature from 473 to 773 K. The surface of the catalytically active phase decreases resulting in a catalyst activity drop. In nitrostyrene hydrogenation, selectivity of Pt based catalysts decreases when the Pt particle size increases.[38]

Very high selectivity of 97% toward 3-VA displayed by Pt/ZnO reduced at 573 K (Table 2) is in line with the results reported earlier for Pt−Zn/HPS catalysts[20] where a similar level of selectivity was obtained. At the same time, activity of the latter was somewhat lower being about 10^3 $mol_{3\text{-}NS}\ mol_{Pt}^{-1}\ h^{-1}$. It is quite clear from the reported data that activity of these selective Pt catalysts was much higher than the one displayed by Au/TiO2 even taking into account three-fold lower hydrogen pressure.[14]

Contrary to Pt/ZnO catalyst, the benchmark Pt/Al_2O_3 and Pt/C catalyzed exclusively the formation of 3-ethylaniline (3-EA) (Table 2). 3-EA is produced from 3-NS either through 3-ethylnitrobenzene (pathways **1** and **2** in Scheme 1) or through 3-VA (pathways **3** and **4**). The observed difference in the reaction pathways can be attributed to a difference in modes of nitrostyrene adsorption on Pt active sites. Boronat et al.[39] studied adsorption of nitrostyrene on Au/TiO_2. They found that 3-NS can be adsorbed and activated on an isolated Au nanoparticle either through NO_2 or C═C group. On an Au nanoparticle supported on TiO_2, however, only selective 3-NS adsorption through the NO_2 group occurs.

To study further the support influence on the catalyst behavior, Pt nanoparticles were supported on different metal

DOI: 10.1021/acs.iecr.5b02113
Ind. Eng. Chem. Res. 2015, 54, 8659−8669

Table 3. Catalytic Results in the Liquid-Phase Hydrogenation of 3-NS to 3-VA over Supported Pt Catalysts with a Series of Solvent. Reaction Conditions: 348 K, 10 bar, 3-NS/Pt Molar Ratio = 150 $mol_{3\text{-}NS}$ mol_{Pt}^{-1}

solvent	dielectric constant (−)	solubility (mole fraction) × 10^4	$S_{3\text{-}VA(XNS=99\%)}$ (%)	initial activity ($mol_{3\text{-}NS}$ mol_{Pt}^{-1} h^{-1}) × 10^{-3}
toluene	2	3.2[a]	75	0.62
tetrahydrofuran	8	2.9[a]	81	0.43
isopropanol	18	2.7[a]	83	0.67
butanol	19		84	0.84
ethanol	24	2.1[a]	97	1.56
methanol	33		98	0.76
MeOH+EtOH			98	1.01
acetonitrile	37		93	0.17
ACN+EtOH			96	0.26

[a]From ref 46 at 10 bar of hydrogen pressure at 298 K.

oxides (MgO, CeO_2, TiO_2, and Fe_2O_3) and tested in 3-NS hydrogenation (Table 2). It was observed that none of the synthesized catalysts is as selective as Pt/ZnO at high conversion >99%. Beier et al.[40] also demonstrated that the reaction pathway of nitrostyrene hydrogenation over Pt nanoparticles can change depending on the support used. Reducible supports, such as TiO_2, Fe_2O_3, or ZnO, lead to a higher selectivity toward of 3-VA, whereas inert ones, such as Al_2O_3 or C, promoted reduction of both vinyl and nitro functionalities.

Choice of the Solvent. With the advent of green processes, the impact of the solvent on the environment, apart from its influence on the catalysis, is of great importance.[41−44] A range of parameters such as polarity, acidity, H_2 solubility, competitive adsorption on the catalyst surface, and mass transfer effects may be responsible of the solvent influence on catalytic behavior.[41−44]

The dielectric constant (also called relative permittivity $\varepsilon_r = \varepsilon/\varepsilon_o$ where ε_o is the permittivity of vacuum) plays an important role in the characterization of solvents, useful for the measurement of solvent polarity (i.e., the higher ε_r the higher is its polar character). This parameter was used in analysis of cinnamaldehyde hydrogenation[44] where it was demonstrated that catalytic behavior of 5%Ru/Y was strongly influenced by the used solvent correlating with solvent polarity. The catalyst was most active in alcohols and relatively inactive in dipolar and apolar solvents. Enantioselectivity in hydrogenation of ethyl benzoylformate[45] and 1,2-propanedione[46] was related to the solvent polarity using the dielectric constant by applying the Kirkwood treatment of the transition state theory.

More recent quantitative attempts to address the solvent effects on the total conversion and the product selectivity in hydrogenation of acetophenone were done by Arai and coworkers[42] by considering solvatochromic solvent parameters such as hydrogen-bond-donation capability (α), hydrogen-bond-acceptance capability (β), and the polarity/polarizability index (π^*). Rh/C activity was correlated with hydrogen-bond-donation capability for Rh/C, while hydrogen-bond-acceptance (HBA) capacity was seen as the governing parameter for Rh/Al_2O_3. These results pointed out that different types of interactions, namely between the carbonyl group of the substrate and the solvent molecules through hydrogen bonding for Rh/C and between the solvent molecules and the catalyst surface for Rh/Al_2O_3, are responsible for the solvent effects.

Only a few studies on the solvent role in nitroarene hydrogenation have been found in the literature.[47,48] In the present work, 3-NS hydrogenation over Pt/ZnO catalyst in a series of organic solvents was studied (Table 3). The 3-VA selectivity is higher in a more polar reaction medium following the trend: ethanol ≈ methanol > acetonitrile > butanol > isopropanol > tetrahydrofuran > toluene.

Overhydrogenation to ethylaniline (∼25%) was observed at high 3-NS conversions (>99%) in toluene over Pt/ZnO, although this solvent is considered as the solvent of choice for 3-NS hydrogenation over Pt- and Au-based catalysts.[49,50] The polarity of the solvent characterized by the dielectric constant seems to play an important role: the selectivity to 3-VA increases with the dielectric constant of alcohols. In particular, lower selectivity is observed in isopropanol as compared to butanol, ethanol, and methanol.

Figueras et al. observed that the rate of nitrobenzene hydrogenation depends on the supply of hydrogen to the Pt surface.[51] According to this study, the catalyst activity is higher in ethanol, where hydrogen has higher solubility, than in acetonitrile. Ethanol added to acetonitrile shows a net activity improvement from 170 to 260 $mol_{3\text{-}NS}$ mol_{Pt}^{-1} h^{-1}.

The experimental data in the current work could not be correlated directly with the hydrogen solubility. At the same time, the activity did not show a dependence on dielectric constant or solvatochromic solvent parameters used in ref 42, pointing out that some other parameters are responsible for high activity in ethanol, which is the best solvent for selective hydrogenation of 3-NS to 3-VA over Pt/ZnO among all studied solvents.

Catalyst Stability. Deactivation of catalysts during nitroarene hydrogenation due to metal leaching,[52] sintering,[53] and coking[54] is widely reported. To monitor the presence of any of these phenomena, stability of the Pt/ZnO catalyst was evaluated over consecutive runs. The obtained data demonstrate that the catalyst activity is stable (1560 $mol_{3\text{-}NS}$ mol_{Pt}^{-1} h^{-1}) after two consecutive reaction cycles with constant 3-VA selectivity ($S_{3\text{-}VA}$ = 97%) at conversion >99%.

Kinetic Modeling. Prior to kinetic modeling an apparent reaction order in hydrogen was calculated giving a value of 0.84. This observation rules out models that can give a maximum reaction order of 0.5 such as models with competitive or noncompetitive dissociative adsorption of hydrogen and addition of the first hydrogen atom as a rate-determining step.

For kinetic modeling, besides a substantially simplified reaction network (Scheme 2) as compared to Scheme 1 and essentially considering hydrogenation of 3-NS to 3-ENB as well as 3-VA, it was decided to incorporate molecular adsorption of hydrogen on the sites distinct from the sites for adsorption of bulky organic species. Such approach can give a fractional reaction order in hydrogen close to unity. The reaction mechanism takes the form

DOI: 10.1021/acs.iecr.5b02113
Ind. Eng. Chem. Res. 2015, 54, 8659−8669

	$N^{(1)}$	$N^{(2)}$	$N^{(3)}$
(1) $Z' + H_2 \equiv Z'H_2$	3	1	1
(2) $Z + A \equiv ZA$	1	1	0
(3) $ZA + Z'H_2 \rightarrow Z' + ZI$	1	0	0
(3′) $ZI + 2Z'H_2 \rightarrow$ (fast)$2Z' + ZB + 2H_2O$	1	0	0
(4) $ZA + Z'H_2 \rightarrow Z' + ZC$	0	1	0
(5) $ZB + Z'H_2 \rightarrow Z' + ZD$	0	0	1
(6) $ZB \equiv Z + B$	1	0	−1
(7) $ZC \equiv Z + C$	0	1	0
(8) $ZD \equiv Z + D$	0	0	1

$$N^{(1)}: A + 3H_2 \rightarrow B + 2H_2O;\ N^{(2)}: A + H_2 \rightarrow C,\ N^{(3)}: B + H_2 \rightarrow D \tag{7}$$

Components A, B, C, and D denote 3-NS, 3-aminostyrene (3-VA), 3-ethylnitrobenzene (3-ENB), and 3-ethylaniline (3-EA), respectively, while Z stands for a surface site, and I represents intermediates in hydrogenation of 3-NS to 3-VA. Steps 1, 2, 6, 7, and 8 are quasiequilibria, while step 3′ is a fast one.

Scheme 2. Simplified Reaction Scheme for the 3-Nitrosytrene Hydrogenation

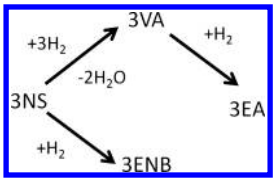

The modeling of kinetics was based on the theory of complex reactions.[55] The elementary steps in eq 7 can be described by three different reaction routes, that is, sets of stoichiometric numbers of the reaction steps. Elementary reactions are grouped in steps, and chemical equations of steps contain reactants, reaction intermediate species, and reaction products. A set of stoichiometric numbers of the steps is defined as a reaction route. Reaction routes are essentially different, and it is impossible to obtain one route through multiplication of another route by a number, although their respective overall reactions can be identical. The number of basic routes, P, is determined by $P = S + W - I$, where S is the number of steps, W is the number of balance equations, and I is the number of reaction intermediates. Balance equations can determine the relationship between intermediates. On the right-hand side of the equations of the steps, stoichiometric numbers for the three routes are given. These numbers are selected in such a way that the overall chemical equations do not contain intermediates. According to the rule of Horiuti-Temkin, the number of independent routes can be determined by subtracting from the number of steps equal to 9 (including 3′) in the mechanism above, number of intermediates equal to eight including the empty sites (Z′, $Z'H_2$, Z, ZI, ZA, ZB, ZC, ZD), and adding the number of balance equations. In fact, since the step 3′ is considered to be fast, concentration of intermediate I on the surface can be neglected, leading to eight steps and seven intermediates. In eq 7, there are two balance equations, which are related to the concentration of intermediates on different types of sites. Following the rule of Horiuti-Temkin, it can be concluded that there are three independent reaction routes.

A straightforward derivation of kinetic equations gives for the reaction rate $r^{(1)}$ along the first route $N^{(1)}$

$$r^{(1)} = k_3\theta_A\theta'_{H_2} = \frac{k_3K_2C_AK_1P_{H_2}}{(1 + K_2C_A + C_B/K_6 + C_C/K_7 + C_D/K_8)(1 + K_1P_{H_2})} \tag{8}$$

defining it through step 3, which can be considered as the one limiting the rate in this route. In eq 11, θ_A stands for coverage of species A, and θ'_{H_2} is the coverage of hydrogen.

The rate along the second route is defined in a similar fashion:

$$r^{(2)} = k_4\theta_A\theta'_{H_2} = \frac{k_4K_2C_AK_1P_{H_2}}{(1 + K_2C_A + C_B/K_6 + C_C/K_7 + C_D/K_8)(1 + K_1P_{H_2})} \tag{9}$$

while the rate along the third route is expressed through step 5:

$$r^{(3)} = k_5\theta_B\theta'_{H_2} = \frac{k_5K_6^{-1}C_BK_1P_{H_2}}{(1 + K_2C_A + C_B/K_6 + C_C/K_7 + C_D/K_8)(1 + K_1P_{H_2})} \tag{10}$$

Finally, the generation rates of compounds can be written as

$$-\frac{dC_A}{dt} = r^{(1)} + r^{(2)};\ \frac{dC_B}{dt} = r^{(1)} - r^{(2)};\ \frac{dC_C}{dt} = r^{(2)};\ \frac{dC_D}{dt} = r^{(3)} \tag{11}$$

The rates from eqs 8−11 contain rate constants k_3, k_{-4}, or k_5, and equilibrium constants K_1, K_2, K_6, K_7, or K_8, which were estimated by numerical data fitting. To this end, the systems of differential eqs 8−11 portraying the kinetic model were solved numerically in the parameter estimations with the backward difference method by minimization of the sum of residual squares, SRS, with nonlinear regression analysis using the Simplex and Levenberg−Marquardt optimization algorithms

DOI: 10.1021/acs.iecr.5b02113
Ind. Eng. Chem. Res. 2015, 54, 8659−8669

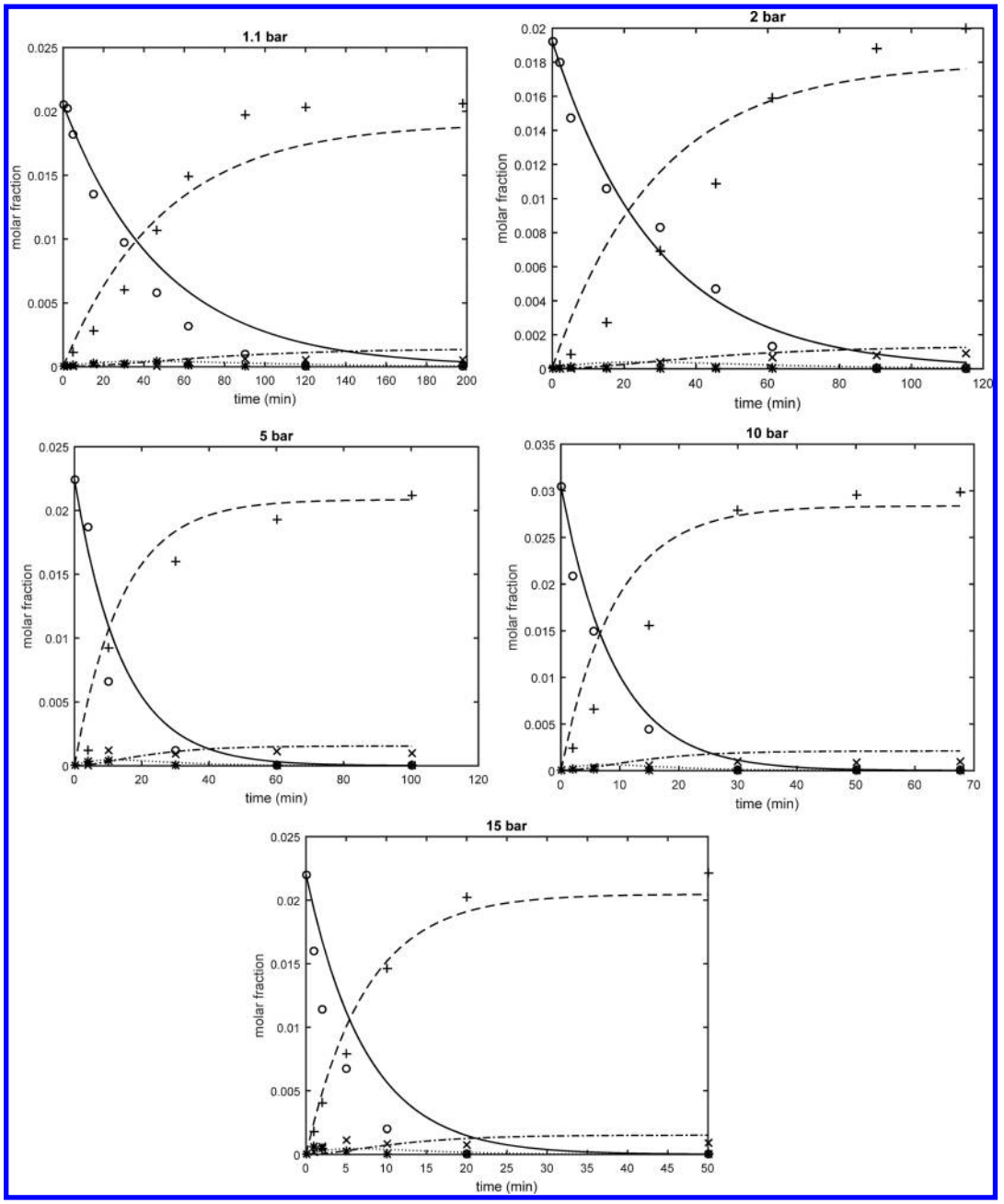

Figure 5. Hydrogenation of nitrostyrene at T = 75 °C in ethanol at Pt/NS ratio = 150 and different hydrogen pressure. ENB, ∗ (experiments) and ··· (calculations); EA, × (experiments) and -·-·- (calculations); NS, ○ (experiments) and − (calculations); VA, + (experiments) and ------ (calculations).

implemented in the software Modest.[56] The sum of squares was minimized using a step size of 0.1 and a value of 1×10^{-6} for both the absolute and relative tolerances of the Simplex and Levenberg−Marquardt optimizer, starting with Simplex and thereafter switching to Levenberg−Marquardt. The closeness of data and model-predicted values were measured with the sum of residual squares and degree of explanation, R^2.[55,56]

Preliminary calculations demonstrated that $1 \gg (K_2C_A + C_B/K_6 + C_C/K_7 + C_D/K_8)$ allowing some simplifications in the rate equations resulting in first-order expressions for organic compounds. Finally, renormalization of the concentrations to their relative values resulted in the rate equations that were used for data fitting:

$$r^{(1)} = \frac{k'_3(C_A/C_A{}^0)K_1P_{H_2}}{(1 + K_1P_{H_2})};\quad r^{(2)} = \frac{k'_4(C_A/C_A{}^0)K_1P_{H_2}}{(1 + K_1P_{H_2})};$$
$$r^{(3)} = \frac{k'_5(C_B/C_A{}^0)K_1P_{H_2}}{(1 + K_1P_{H_2})} \quad (12)$$

where k'_3−k'_5 are lumped constants, which include adsorption coefficients. The estimated parameter values are shown in Table S1.

A comparison of predictions of the kinetic model with experimental data for hydrogenation is presented in Figure 5 demonstrating that a good data fitting was achieved. The model had the value of residual sum of squares 0.49 and degree of explanation R^2 = 97.24%. The parameters k'_4 and k'_5 are not that

DOI: 10.1021/acs.iecr.5b02113
Ind. Eng. Chem. Res. 2015, 54, 8659−8669

well-defined, which is related to low concentrations of by-products compared to the main reactants 3-NS and 3-VA.

An interesting feature in Figure 5 is that calculations slightly deviate from experimental data at 1.1 and 2 bar, which display some sort of autocatalytic behavior not seen at other pressures and not incorporated in the modeling. Typically, hydrogenation of aromatic nitrocompounds does not display these feactures; therefore, this unusual behavior will require acquisition of additional data and a separate kinetic analysis, which is ongoing.

Hydrogenation of Functionalized Nitroarenes. The performance of Pt/ZnO is tested in hydrogenation of functionalized nitroarenes considering a series of 3-substituted ($-CH_3$, $-H$, $-Cl$, $-Br$, $-COOH$, and $-NO_2$) nitrobenzenes. The high selectivity toward the corresponding functionalized aminoarene (AA) ($S_{AA} \geq 97\%$) is obtained at close to full nitroarene conversion. The results (Table 4) suggest an increased transformation rate, as compared to nitrobenzene, for the electron-withdrawing substituents (e.g., $-Cl$, $-Br$, $-COOH$, $-NO_2$). For electron-donating substituents (e.g., $-CH_3$, $-CH{=}CH_2$), the catalyst activity is lower as compared to nitrobenzene. This is consistent with the nucleophilic reaction mechanism proposed elsewhere for hydrogenation of 4-substituted nitroarenes over Pt nanoparticles[38,57] and 3-substituted nitroarenes over Ir nanoparticles.[58] The obtained results illustrate the potential of the Pt/ZnO catalytic system for selective reduction of various nitroarenes.

Table 4. Catalytic Results in the Liquid-Phase Hydrogenation of a Series of 3-Substituted Nitroarenes (NA) to 3-Substituted Aminoarenes (AA) over Pt/ZnO. Reaction Conditions: 348 K; 10 bar; NA/Pt Molar Ratio = 150 $mol_{3\text{-}NA}$ mol_{Pt}^{-1} in Ethanol

Name of nitroarene	Formula	$S_{AA(X_{NA}=99\%)}$ (%)	Initial activity (mol_{NA} mol_{Pt}^{-1} s^{-1}) × 10^{-3}
Nitrotoluene	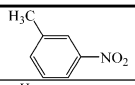	100	1.14
Nitrobenzene	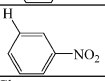	100	1.24
Chloronitrobenzene	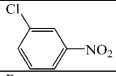	98	1.34
Bromonitrobenzene	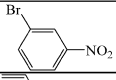	99	1.41
Nitrostyrene	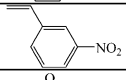	97	1.56
Nitrobenzoic acid	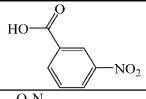	100	1.94
Dinitrobenzene	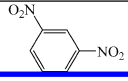	99	2.69

The combination of stability and selectivity represents a significant development in terms of potential application of Pt/ZnO for industrial implementation.

CONCLUSIONS

Pt/ZnO catalyst with a mean Pt nanoparticle size 2.5 ± 0.3 nm promotes the liquid-phase hydrogenation of 3-NS mainly to 3-VA ($S_{3\text{-}VA} = 97\%$) at full 3-NS conversion ($T = 348$ K, $P = 10$ bar) due to PtZn alloy formation. The reaction selectivity is maintained without detectable catalyst deactivation over repeated reaction runs. Benchmark Pt/Al_2O_3 and Pt/C catalysts exhibited a higher TOF (21.7 s^{-1} and 18.4 s^{-1}, respectively) as compared to Pt/ZnO (12.4 s^{-1}) but generate solely over hydrogenated 3-EA byproduct. Different metal oxides supports (MgO, CeO_2, TiO_2, and Fe_2O_3) were tested, but none of them showed selectivity as high as with Pt/ZnO.

For a series of solvents of different polarity (ethanol, methanol, acetonitrile, butanol, isopropanol, tetrahydrofuran, and toluene) the highest yield was achieved with ethanol.

The hydrogenation of a series of 3-substituted ($-CH_3$, $-H$, $-Cl$, $-Br$, $-CHCH_2$, $-COOH$, and $-NO_2$) nitroarenes over Pt/ZnO resulted in almost exclusive formation of corresponding aminocompounds ($S_{AA} \geq 97\%$) with an appreciably high activity (up to 2.69 × 10^3 $mol_{3\text{-}NA}$ mol_{Pt}^{-1} h^{-1}).

Kinetic modeling of 3-NS hydrogenation over Pt/ZnO was successfully performed being consistent with the parallel-consecutive reaction network of 3-NS hydrogenation to 3-ENB as well as to 3-VA considering molecular nondissociative adsorption of hydrogen on the sites distinct from the sites for the adsorption of bulky organic species.

The findings of this work demonstrate a potential of Pt/ZnO as an efficient catalyst for selective hydrogenation of functionalized nitroarenes.

ASSOCIATED CONTENT

Supporting Information

The Supporting Information is available free of charge on the ACS Publications website at DOI: 10.1021/acs.iecr.5b02113.

Calculated values of kinetic parameters and XRD data for Pt/ZnO (PDF)

AUTHOR INFORMATION

Corresponding Authors

*E-mail: lioubov.kiwi-minsker@epfl.ch.

*E-mail: dmurzin@abo.fi.

Notes

The authors declare no competing financial interest.

ACKNOWLEDGMENTS

The participation of I. Cornu and Z. Petrova in the catalyst testing is highly appreciated. The authors are grateful to N. Xanthopoulos and M. Crespo-Quesada for their contribution to the catalyst characterization. This work was funded by the European Union through the Seventh Framework Programme (project POLYCAT; Grant No. CP-IP 246095-2), Swiss Science Foundation (Grant No. 200020_149869), and Russian Science Foundation (Grant No. 15-19-20023).

REFERENCES

(1) Chen, B.; Dingerdissen, U.; Krauter, J. G. E.; Lansink Rotgerink, H. G.J.; Möbus, K.; Ostgard, D. J.; Panster, P.; Riermeier, T. H.; Seebald, S.; Tacke, T.; Trauthwein, H. New Developments in Hydrogenation Catalysis Particularly in Synthesis of Fine and Intermediate Chemicals. *Appl. Catal., A* **2005**, *280*, 17−46.

(2) Cárdenas-Lizana, F.; Berguerand, C.; Yuranov, I.; Kiwi-Minsker, L. Chemoselective Hydrogenation of Nitroarenes: Boosting Nanoparticle Efficiency by Confinement within Highly Porous Polymeric Framework. *J. Catal.* **2013**, *301*, 103−111.

(3) Han, X.; Zhou, R.; Lai, G.; Zheng, X. Influence of Support and Transition Metal (Cr, Mn, Fe, Co, Ni and Cu) on the Hydrogenation of *p*-Chloronitrobenzene over Supported Platinum Catalysts. *Catal. Today* **2004**, *93*−*95*, 433−437.

DOI: 10.1021/acs.iecr.5b02113
Ind. Eng. Chem. Res. 2015, 54, 8659−8669

(4) Blaser, H. U.; Malan, C.; Pugin, B.; Spindler, F.; Steiner, H.; Studer, M. Selective Hydrogenation for Fine Chemicals: Recent Trends and New Developments. *Adv. Synth. Catal.* **2003**, *345*, 103−151.
(5) Blaser, H.-U. Developing Catalysts and Catalytic Processes with Industrial Relevance. *Chimia* **2010**, *64*, 65−68.
(6) Exner, C.; Pfaltz, A.; Studer, M.; Blaser, H.-U. Heterogeneous Enantioselective Hydrogenation of Activated Ketones Catalyzed by Modified Pt-Catalysts: A Systematic Structure-Selectivity Study. *Adv. Synth. Catal.* **2003**, *345*, 1253.
(7) Ferguson, J.; Zeng, F.; Alwis, N.; Alper, H. Synthesis of 2(1*H*)-Quinolinones *via* Pd-Catalyzed Oxidative Cyclocarbonylation of 2-Vinylanilines. *Org. Lett.* **2013**, *15*, 1998−2001.
(8) Kim, J. H.; Park, J. H.; Chung, Y. K.; Park, K. H. Ruthenium Nanoparticle-Catalyzed, Controlled and Chemoselective Hydrogenation of Nitroarenes using Ethanol as a Hydrogen Source. *Adv. Synth. Catal.* **2012**, *354*, 2412−2418.
(9) Takeichi, T.; Thongpradith, S.; Hirai, S.; Takiguchi, T.; Kawauchi, T. Syntheses of Novel Benzoxazines Having Vinyl Groups and Thermal Properties of the Thermosets. *High Perform. Polym.* **2012**, *24*, 765−774.
(10) Xu, Z.; Wang, S.; Wang, L.; Fang, Z.; Wang, X. Preparation and Pyroelectric Properties of Poly(pentafluorostyrene)-r-Poly(4-vinylaniline) Copolymer Films. *Macromol. Symp.* **2008**, *261*, 144−147.
(11) Haber, F. *Elektrochem* **1898**, *22*, 506.
(12) Corma, A.; Concepcion, P.; Serna, P. A Different Reaction Pathway for the Reduction of Aromatic Nitro Compounds on Gold Catalyst. *Angew. Chem., Int. Ed.* **2007**, *46*, 7266−7269.
(13) Serna, P.; Concepción, P.; Corma, A. Design of Highly Active and Chemoselective Bimetallic Gold-Platinum Hydrogenation Catalysts through Kinetic and Isotopic Studies. *J. Catal.* **2009**, *265*, 19−25.
(14) Corma, A.; Serna, P. Chemoselective Hydrogenation of Nitro Compounds with Supported Gold Catalysts. *Science* **2006**, *313*, 332−334.
(15) Sheldon, R. A. Fundamentals of green Chemistry: Efficiency in Reaction Design. *Chem. Soc. Rev.* **2012**, *41*, 1437−1451.
(16) Silvestre-Albero, J.; Sepúlveda-Escribano, J.; Rodrıguez-Reinoso, F.; Anderson, J. A. Influence of Zn on the Characteristics and Catalytic Behavior of TiO_2-Supported Pt catalysts. *J. Catal.* **2004**, *223*, 179−190.
(17) Crespo-Quesada, M.; Grasemann, M.; Semagina, N.; Renken, A.; Kiwi-Minsker, L. Kinetics of the Solvent-Free Hydrogenation of 2-Methyl-3-Butyn-2-Ol over a Structured Pd-Based Catalyst. *Catal. Today* **2009**, *147*, 247−254.
(18) Blaser, H. U.; Steiner, H.; Studer, M. Selective Catalytic Hydrogenation of Functionalized Nitroarenes: An Update. *ChemCatChem* **2009**, *1*, 210−221.
(19) Yarulin, A.; Berguerand, C.; Yuranov, I.; Cardenas-Lizana, F.; Prokopyeva, I.; Kiwi-Minsker, L. Pt-Zn Nanoparticles Supported on Porous Polymeric Matrix for Selective 3-Nitrostyrene Hydrogenation. *J. Catal.* **2015**, *321*, 7−12.
(20) Consonni, M.; Jokic, D.; Murzin, D. Y.; Touroude, R. High Performances of Pt/ZnO Catalysts in Selective Hydrogenation of Crotonaldehyde. *J. Catal.* **1999**, *188*, 165−175.
(21) Dollimore, D.; Heal, G. R. Pore-size Distribution in Typical Adsorbent Systems. *J. Colloid Interface Sci.* **1970**, *33*, 508−519.
(22) Hopfengärtner, G.; Borgmann, D.; Rademacher, I.; Wedler, G.; Hums, E.; Spitznagel, G. W. XPS Studies of Oxidic Model Catalysts: Internal Standards and Oxidation Numbers. *J. Electron Spectrosc. Relat. Phenom.* **1993**, *63*, 91−116.
(23) Bruehwiler, A.; Semagina, N.; Grasemann, M.; Renken, A.; Kiwi-Minsker, L.; Saaler, A.; Lehmann, H.; Bonrath, W.; Roessler, F. Three-Phase Catalytic Hydrogenation of a Functionalized Alkyne: Mass Transfer and Kinetic Studies with in Situ Hydrogen Monitoring. *Ind. Eng. Chem. Res.* **2008**, *47*, 6862−6869.
(24) Macdonald, F.; Lide, D. R. CRC Handbook of Chemistry and Physics: From Paper to Web. *Abstr. Pap. Am. Chem. Soc.* **2003**, *225*, U552−U552.
(25) Cubeiro, M. L.; Fierro, J. L.G. Selective Production of Hydrogen by Partial Oxidation of Methanol over ZnO-Supported Palladium Catalysts. *J. Catal.* **1998**, *179*, 150−162.
(26) Hidalgo-Carrillo, J.; Aramendía, M. A.; Marinas, M.; Marinas, J. M.; Urbano, F. J. Support and Solvent Effects on the Liquid-Phase Chemoselective Hydrogenation of Crotonaldehyde over Pt Catalysts. *Appl. Catal., A* **2010**, *385*, 190−200.
(27) Liu, X.; Guo, Y.; Xu, W.; Wang, Y.; Gong, X.; Guo, Y.; Guo, Y.; Lu, G. Catalytic Properties of Pt/Al_2O_3 Catalysts in the Aqueous Phase Reforming of Ethylene Glycol: Effect of the Alumina Support. *Kinet. Catal.* **2011**, *52*, 817−822.
(28) Borgna, A.; Garetto, T. F.; Apesteguia, C. R.; Le Normand, F.; Moraweck, B. Sintering of Chlorinated Pt/Gamma-Al_2O_3 Catalysts: An In Situ Study by X-Ray Absorption Spectroscopy. *J. Catal.* **1999**, *186*, 433−441.
(29) Le Normand, F.; Borgna, A.; Garetto, T. F.; Apesteguia, C. R.; Moraweck, B. Redispersion of Sintered Pt/Al_2O_3 Naphtha Reforming Catalysts: An *In Situ* Study Monitored by X-Ray Absorption Spectroscopy. *J. Phys. Chem.* **1996**, *100*, 9068−9076.
(30) Wang, D.; Ammari, F.; Touroude, R.; Su, D. S.; Schlögl, R. Promotion Effect in Pt−ZnO Catalysts for Selective Hydrogenation of Crotonaldehyde to Crotyl Alcohol: A Structural Investigation. *Catal. Today* **2009**, *147*, 224−230.
(31) Ammari, F.; Lamotte, J.; Touroude, R. An Emergent Catalytic Material: Pt/ZnO Catalyst for Selective Hydrogenation of Crotonaldehyde. *J. Catal.* **2004**, *221*, 32−42.
(32) Shyu, J. Z.; Otto, K. Identification of Platinum Phases on γ-Alumina by XPS. *Appl. Surf. Sci.* **1988**, *32*, 246−252.
(33) Amorim, C.; Yuan, G.; Patterson, P. M.; Keane, M. A. Catalytic Hydrodechlorination over Pd Supported on Amorphous and Structured Carbon. *J. Catal.* **2005**, *234*, 268.
(34) Trueba, M.; Trasatti, S. P. γ-Alumina as a Support for Catalysts: A Review of Fundamental Aspects. *Eur. J. Inorg. Chem.* **2005**, *2005*, 3393.
(35) Veldurthi, S.; Shin, C.-H.; Joo, O. S.; Jung, K. D. Promotional Effects of Cu on Pt/Al_2O_3 and Pd/Al_2O_3 Catalysts during n-Butane Dehydrogenation. *Catal. Today* **2012**, *185*, 88−93.
(36) Aksoylu, A. E.; Faria, J. L.; Pereira, M. F. R.; Figueiredo, J. L.; Serp, P.; Hierso, J.-C.; Feurer, R.; Kihn, Y.; Kalck, P. Highly Dispersed Activated Carbon Supported Platinum Catalysts Prepared by OMCVD: A Comparison with Wet Impregnated Catalysts. *Appl. Catal., A* **2003**, *243*, 357−365.
(37) Lim, B.; Jiang, M.; Tao, J.; Camargo, P. H. C.; Zhu, Y.; Xia, Y. Shape-Controlled Synthesis o f Pd Nanocrystals In Aqueous Solutions. *Adv. Funct. Mater.* **2009**, *19*, 189−200.
(38) Cardenas-Lizana, F.; Berguerand, C.; Yuranov, I.; Kiwi-Minsker, L. Chemoselective Hydrogenation of Nitroarenes: Boosting Nanoparticle Efficiency by Confinement within Highly Porous Polymeric Framework. *J. Catal.* **2013**, *301*, 103−111.
(39) Boronat, M.; Concepción, P.; Corma, A.; González, S.; Illas, F.; Serna, A. A Molecular Mechanism for the Chemoselective Hydrogenation of Substituted Nitroaromatics with Nanoparticles of Gold on TiO_2 Catalysts: A Cooperative Effect between Gold and the Support. *J. Am. Chem. Soc.* **2007**, *129*, 16230−16237.
(40) Beier, M. J.; Andanson, J.-M.; Baiker, A. Tuning the Chemoselective Hydrogenation of Nitrostyrenes Catalyzed by Ionic Liquid-Supported Platinum Nanoparticles. *ACS Catal.* **2012**, *2*, 2587−2595.
(41) Curzons, A. D.; Constable, D. C.; Cunningham, V. L. Solvent Selection Guide: A Guide to the Integration of Environmental, Health and Safety Criteria into the Selection of Solvents. *Clean Technol. Environ. Policy* **1999**, *1*, 82−90.
(42) Yoshida, H.; Onodera, Y.; Fujita, S.-i.; Kawamori, H.; Arai, M. Solvent Effects in Heterogeneous Selective Hydrogenation of Acetophenone: Differences between Rh/C and Rh/Al_2O_3 Catalysts and the Superiority of Water as a Functional Solvent. *Green Chem.* **2015**, *17*, 1877−1883.
(43) Yoshida, H.; Kato, K.; Wang, J.; Meng, X.; Narisawa, S.; Fujita, S.-i.; Wu, Z.; Zhao, F.; Arai, M. Hydrogenation of Nitrostyrene with a Pt/TiO2 Catalyst in CO_2. Dissolved Expanded Polar and Nonpolar Organic Liquids: Their Macroscopic and Microscopic Features. *J. Phys. Chem. C* **2011**, *115*, 2257−2267.

DOI: 10.1021/acs.iecr.5b02113
Ind. Eng. Chem. Res. 2015, 54, 8659−8669

(44) Hajek, J.; Kumar, N.; Mäki-Arvela, P.; Salmi, T.; Murzin, D.Yu. Selective Hydrogenation of Cinnamaldehyde over Ru/Y Zeolite. *J. Mol. Catal. A: Chem.* **2004**, *217*, 145−154.
(45) Martin, G.; Mäki-Arvela, P.; Murzin, D.Yu.; Salmi, T. Solvent Effects in Enantioselective Hydrogenation of Ethyl Benzoylformate. *Catal. Lett.* **2013**, *143*, 1051−1060.
(46) Toukoniitty, E.; Mäki-Arvela, P.; Kuusisto, J.; Nieminen, V.; Päivärinta, J.; Hotokka, M.; Salmi, T.; Murzin, D.Yu. Solvent Effects in Enantioselective Hydrogenation of 1-Phenyl−1,2-Propanedione. *J. Mol. Catal. A: Chem.* **2003**, *192*, 135−151.
(47) Cárdenas-Lizana, F.; Gómez-Quero, S.; Keane, M. A. Exclusive Production of Chloroaniline from Chloronitrobenzene over Au/TiO_2 and Au/Al_2O_3. *ChemSusChem* **2008**, *1*, 215−221.
(48) Pandarus, V.; Ciriminna, R.; Béland, F.; Pagliaro, M. A New Class of Heterogeneous Platinum Catalysts for the Chemoselective Hydrogenation of Nitroarenes. *Adv. Synth. Catal.* **2011**, *353*, 1306−1316.
(49) Fujita, S.-I.; Yoshida, H.; Asai, K.; Meng, X.; Arai, M. Selective Hydrogenation of Nitrostyrene to Aminostyrene over Pt/TiO_2 Catalysts: Effects of Pressurized Carbon Dioxide and Catalyst Preparation Conditions. *J. Supercrit. Fluids* **2011**, *60*, 106−112.
(50) Serna, P.; Boronat, M.; Corma, A. Tuning the Behavior of Au and Pt Catalysts for the Chemoselective Hydrogenation of Nitroaromatic Compounds. *Top. Catal.* **2011**, *54*, 439−446.
(51) Figueras, F.; Coq, B. Hydrogenation and Hydrogenolysis of Nitro-, Nitroso-, Azo-, Azoxy- and Other Nitrogen-Containing Compounds on Palladium. *J. Mol. Catal. A: Chem.* **2001**, *173*, 223−230.
(52) Yeong, K. K.; Gavriilidis, A.; Zapf, R.; Hessel, V. Catalyst Preparation and Deactivation Issues for Nitrobenzene Hydrogenation in a Microstructured Falling Film Reactor. *Catal. Today* **2003**, *81*, 641−651.
(53) Du, Y.; Chen, H.; Chen, R.; Xu, N. Synthesis of *p*-Aminophenol From *P*-Nitrophenol over Nano-Sized Nickel Catalysts. *Appl. Catal., A* **2004**, *277*, 259−264.
(54) Diao, S.; Qian, W.; Luo, G.; Wei, F.; Wang, Y. Gaseous Catalytic Hydrogenation of Nitrobenzene to Aniline in a Two-Stage Fluidized Bed Reactor. *Appl. Catal., A* **2005**, *286*, 30−35.
(55) Murzin, D.; Salmi, T. *Catalytic Kinetics*; Elsevier: Amsterdam, 2005.
(56) Haario, H. *Modest User Guide*; Helsinki: Finland, 2011.
(57) Cárdenas-Lizana, F.; Lamey, D.; Gómez-Quero, S.; Perret, N.; Kiwi-Minsker, L.; Keane, M. A. Selective Three-Phase Hydrogenation of Aromatic Nitro-Compounds over B-Molybdenum Nitride. *Catal. Today* **2011**, *173*, 53−61.
(58) Campos, C.; Torres, C.; Oportus, M.; Peña, M. A.; Fierro, J. L. G.; Reyes, P. Hydrogenation of Substituted Aromatic Nitrobenzenes over 1% 1.0 wt.%Ir/ZrO_2 Catalyst: Effect of Meta Position and Catalytic Performance. *Catal. Today* **2013**, *213*, 93−100.

DOI: 10.1021/acs.iecr.5b02113
Ind. Eng. Chem. Res. 2015, 54, 8659−8669